Polyhedron 119 (2016) 184–193

Contents lists available at ScienceDirect

Polyhedron

journal homepage: www.elsevier.com/locate/poly

Synthesis, structural characterization, stability, antibacterial activity and spectroscopic properties (THz) of five new polynuclear silver(I) complexes with 1,10-phenanthroline derivative and 1,3-bis(diphenylphosphino)propane (dppp)

Yuan Yuan [a], Hong-Liang Han [a], Sen Lin [a], Yang-Zhe Cui [a], Min Liu [b], Zhong-Feng Li [a], Qiong-Hua Jin [a,*], Yu-Ping Yang [c], Zhen-Wei Zhang [d]

[a] Department of Chemistry, Capital Normal University, Beijing 100048, China
[b] The College of Materials Science and Engineering, Beijing University of Technology, Beijing 100022, China
[c] School of Science, Minzu University of China, Beijing 100081, China
[d] Beijing Key Laboratory for Terahertz Spectroscopy and Imaging, Key Laboratory of Terahertz Optoelectronics, Ministry of Education, Department of Physics, Capital Normal University, Beijing 100048, China

ARTICLE INFO

Article history:
Received 21 April 2016
Accepted 24 August 2016
Available online 31 August 2016

Keywords:
Silver(I)
1,3-Bis(diphenylphosphino)propane
Luminescent
Terahertz spectra
Antibacterial activity

ABSTRACT

The reactions of 1,3-bis(diphenylphosphino)propane (dppp) and 1,10-phenanthroline derivative with Ag salts in the mixed solvent of methanol and dichloromethane generate the corresponding complexes, $\{[Ag_2(dppp)_2(phen)_2](BF_4)_2(H_2O)_2\}_n$ (**1**) (dppp = 1,3-bis(diphenylphosphino)propane), $\{[Ag_2(dppp)_2(dmp)_2](CF_3SO_3)_2\}_n$ (**2**), $\{[Ag_2(dppp)_2(dmp)_2](BF_4)\}_n$ (**3**) (dmp = neocuproine), $\{[Ag_2(dppp)_2(Bphen)_2](CF_3SO_3)_2\}_n$ (**4**) and $\{[Ag_2(dppp)_2(Bphen)_2](ClO_4)\}$ (**5**) (Bphen = 4,7-diphenyl-1,10-diazaphenanthrene). All the complexes are characterized by X-ray diffraction, luminescence, ^{31}P, ^{1}H NMR spectroscopy and terahertz (THz) spectra. These five complexes are of dinuclear structures. The topological analysis of simplified underlying nets reveals that complexes **1**–**4** have topologically promising architectures formed through hydrogen bonds (F···H–C) between the C–H groups of aromatic ring and anions. Thermogravimetric analysis (TGA) shows the complexes **1**–**5** possess good thermal stability up to 300 °C.

1. Introduction

The silver(I) coordination polymers have attracted great interest not only for their extensive applications as functional materials, but also for their intriguing architectures [1–3]. Because of their potential applications in the fields of biological activity, catalysis and light emitting devices [4], the mixed IB metal complexes combining bisphosphines (PP) and aromatic diamine ligands have been intensively investigated during past years [4–8]. Only a few examples of silver(I) complexes with similar structures are reported in the literatures so far [9–13]. For examples, the dppp ligand was used to synthesize the $[Ag(dppp)(phen)](BF_4)$ complex [8]. and the ligand dppFc and bis(diphenylphosphanyl)ocarborane were used to synthesize $[Ag(PP)(phen)]^+$ derivatives [10,11]. It is noteworthy that Pettinari et al. have reported the dinuclear silver complexes of general formula $[(AgX)_2(PP)(NN)_2]$ ($X = ClO_4$ or NO_3), which have interesting structural features [8,13,13e]. Furthermore, various functional coordination topologies have been constructed by reaction of silver(I) ions with certain designed spacer ligands [14–18]. This is coupled with the flexibility of silver(I) center in the adoption of different coordination numbers and geometries with noncovalent interactions such as hydrogen bonding and π–π interaction among others [19]. For example, 1D $[Ag_2(\mu\text{-PTA})_2(\mu\text{-suc})]_n{\cdot}2nH_2O$, 2D $[Ag_2(\mu\text{-PTA})_2(\mu_4\text{-adip})]_n{\cdot}2nH_2O$, and 3D $[Ag_2(\mu_4\text{-PTA})(\mu_4\text{-mal})]_n$ [20] have been reported.

In addition, a pronounced attention has been aroused to the investigation of the new bioactive metal–organic framework materials (bioMOFs) combined with construction materials as potential antibacterial materials (e.g., antibacterial coating and antibacterial glass). Meanwhile, scientists are devoted to the synthesis of new silver complexes with the biological activity as possible alternatives to the traditional antibiotics. It is widely known that silver and its simple salts are valid antimicrobial agents. Among all the bioactive metals, silver exhibits the highest toxicity to bacteria, and simultaneously shows a relatively low toxicity to mammal

* Corresponding author. Fax: +86 10 68902320.
E-mail address: jinqh@mail.cnu.edu.cn (Q.-H. Jin).

http://dx.doi.org/10.1016/j.poly.2016.08.038
0277-5387/

cells. A large number of bioactive silver complexes have been reported [20]. It was observed that complexes having weak Ag–N bonds usually exhibit higher bioactivity than complexes possessing strong Ag–P bonds [20]. Antimicrobial activities of complexes with Ag–X (X = P, N) can be tuned by varying the space configuration of silver complexes and the number of silver atom [21]. Following this systematic studies on $[Ag(PP)(NN)]^+$ complexes, we are naturally interested in extending our investigation to analogous heteroleptic silver(I) complexes and expected to obtain the silver(I) complexes possessing bioMOFs. Here, five new polynuclear silver(I) complexes (containing Ag–N and Ag–P bonds) with 1,10-phenanthroline derivative and 1,3-bis(diphenylphosphino) propane (dppp) are synthesized and the antimicrobial properties of these complexes are detected.

Compared with the traditional spectrum technology, terahertz spectrum has a high noise ratio and special properties such as coherence, transient. The application of terahertz time-domain spectroscopy (THz-TDS) gradually developed from the narrow field (information technology, physics, materials) to a wider range of areas (such as chemistry, biology, and medicine areas) [22–25]. Due to its sensitivity, THz spectrum can be used to detect the intermolecular weak interaction such as hydrogen bond, van der Waals force, dipole rotation and vibration transition, the lattice of low-frequency vibration and so on. THz spectroscopy has been utilized to study the structures, configurations and environmental state of compounds by our group [26,27].

In this paper, we report the synthesis and characterization of di- and poly-nuclear silver(I) complexes containing dppp, where the versatility of coordination of silver(I) allows for a variety of coordination modes with the dppp ligand. Complexes **1**–**4** are of topologically promising architectures. The fluorescence spectra and THz-TDS of complexes **1**–**5** have been researched in this article. In addition, complexes **1**–**4** show significant antibacterial activity against the selected strains of Gram-negative (*Escherichia coli*) and Gram-positive (*Bacillus subtilis*, *Staphylococcus aureus*) bacteria.

2. Experimental section

2.1. Materials and measurements

All chemical reagents silver perchlorate ($AgClO_4$), silver tetrafluoroborate ($AgBF_4$), silver trifluoromethanesulfonate ($AgCF_3SO_3$), 1,10-phenanthroline (phen), 4,7-diphenyl-1,10-diazaphenanthrene (Bphen), Neocuproine (dmp), 1,3-bis(diphenylphosphino) propane (dppp) are commercially available and used without further purification. Elemental analyses (C, H, N) were determined on a Elementar Vario MICRO CUBE (Germany) elemental analyzer. Infrared spectra were recorded on a Bruker EQUINOX 55 FT-IR spectrometer using the KBr pellet in the range of 400–4000 cm^{-1}. Excitation and emission spectra of the solid samples were recorded on an F-4500 fluorescence spectrophotometer at room temperature. ^1H and ^{31}P NMR was recorded at room temperature with a Varian VNMRS 600 MHz and 243 MHz spectrometer, respectively. The THz absorption spectra were recorded on the THz time domain device of Capital Normal University of China, based on photoconductive switches for generation and electro-optical crystal detection of the far-infrared light, effective frequency in the range of 0.2–4.0 THz [28,29].

2.2. Preparation of the complexes

2.2.1. Synthesis of $\{[Ag_2(dppp)_2(phen)_2](BF_4)_2(H_2O)_2\}_n$ (**1**)

Dppp (0.2 mmol, 0.0825 g) was added into the stirring solution of $AgBF_4$ (0.2 mmol, 0.0384 g) in a mixture of CH_2Cl_2 (5 ml) and CH_3OH (5 ml) for 5 h at ambient temperature. The insoluble residues were removed by filtration, and the brown filtrate was evaporated slowly at room temperature for about one week to yield white crystals. After phen (0.2 mmol, 0.0361 g) was added into the stirring solution of crystals in mixing of CH_2Cl_2 (5 ml) and CH_3OH (5 ml) for 5 h. The insoluble residues were removed by filtration, and the brown filtrate was evaporated slowly at room temperature for about one week to yield white crystals. Yields: 66%. *Anal.* Calc. for $C_{78}H_{72}Ag_2B_2F_8N_4O_2P_4$: elemental analysis: C, 58.17; H, 4.47; N, 3.48%. Measured value: C, 58.85; H, 4.52; N, 3.47%. IR (cm^{-1}, KBr pellets): 3550w, 3051w, 2908w, 1621m, 1587m, 1570m, 1510s, 1483s, 1434s, 1422s, 1375m, 1309m, 1275s, 1221s, 1142s, 1057vs, 955s, 844s, 820m, 757s, 745s, 730s, 697s, 645m, 547s, 511s, 480s, 444s. ^1H NMR (600 MHz, $CDCl_3$, 298 K): δ = 1.2–1.5 (m, 12H, dppp-$CH_2CH_2CH_2$), 7.2–7.4 (m, with solvent signal peak overlap, dppp-ph), 7.2–7.4 (m, $H^{3,8}$-phen), 7.7 (d, 4H, $H^{5,6}$-phen), 8.2–8.8 (m, 4H, $H^{2,9}$-phen) ppm. ^{31}P NMR (243 MHz, $CDCl_3$): δ = 4.8 (d, J_{Ag-P} = 420 Hz), −5.9 (d, J_{Ag-P} = 233 Hz).

2.2.2. Synthesis of $\{[Ag_2(dppp)_2(dmp)_2](CF_3SO_3)_2\}_n$ (**2**)

Dppp (0.2 mmol, 0.0825 g) and dmp (0.2 mmol, 0.0417 g) were added into the stirring solution of $AgCF_3SO_3$ (0.2 mmol, 0.0514 g) in a mixture of CH_2Cl_2 (5 ml) and CH_3OH (5 ml) for 5 h at ambient temperature. The insoluble residues were removed by filtration, and the brown filtrate was evaporated slowly at room temperature for about a week to yield white crystals. Yields: 70%. *Anal.* Calc. for $C_{84}H_{76}Ag_2F_6N_4O_6P_4S_2$: elemental analysis: C, 57.48; H, 4.33; N, 3.19%. Measured value: C, 57.58; H, 4.42; N, 3.20%. IR(cm^{-1}, KBr pellets): 3434s, 3052s, 2919w, 1967w, 1620s, 1593s, 1556s, 1501vs, 1484vs, 1435vs, 1375s, 1359w, 1271vs, 1222vs, 1145vs, 1099vs, 1030vs, 998s, 956m, 854s, 804m, 783m, 743s, 729s, 698s, 636s, 571m, 548m, 513s, 478m, 445m. ^1H NMR (600 MHz, $CDCl_3$, 298 K): δ = 1.3–1.5 (m, 4H, dppp-$CH_2CH_2CH_2$), 2.3–2.4 (br, 8H, dppp-$CH_2CH_2CH_2$, 12H, dmp-CH_3), 7.2–7.4 (m, with solvent signal peak overlap, dppp-ph, $H^{3,8}$-dmp), 7.6 (br, 4H, $H^{5,6}$-dmp), 7.9–8.1 (m, 4H, $H^{4,7}$-dmp) ppm. ^{31}P NMR (243 MHz, $CDCl_3$): δ = 1.7 (d, J_{Ag-P} = 366 Hz), −5.9 (d, J_{Ag-P} = 235 Hz).

2.2.3. Synthesis of $\{[Ag_2(dppp)_2(dmp)_2](BF_4)\}_n$ (**3**)

Follow a similar procedure as **2**, dppp (0.2 mmol, 0.0825 g) and dmp (0.2 mmol, 0.0417 g) were added into the stirring solution of $AgBF_4$ (0.2 mmol, 0.0384 g) in a mixture of CH_2Cl_2 (5 ml) and CH_3OH (5 ml) for 5 h at ambient temperature. The insoluble residues were removed by filtration, and the brown filtrate was evaporated slowly at room temperature for about one week to yield white crystals. Yields: 70%. *Anal.* Calc. for $C_{83}H_{80}Ag_2B_2F_8N_4OP_4$: elemental analysis: C, 59.94; H, 4.82; N, 3.37%. Measured value: C, 60.09; H, 4.87; N, 3.40%. IR (cm^{-1}, KBr pellets): 3434s, 3051s, 2918s, 1620s, 1591s, 1556s, 1501vs, 1484vs, 1435vs, 1375s, 1306m, 1281m, 1221m, 1156m, 1059vs, 955s, 854s, 807s, 743s, 728m, 697vs, 647s, 548m, 513s, 480s, 444s. ^1H NMR (600 MHz, DMSO, 298 K): δ = 2.3–2.5 (m, 8H, dppp-$CH_2CH_2CH_2$, 12H, dmp-CH_3), 3.3 (br, 4H, dppp-$CH_2CH_2CH_2$), 7.2–7.4 (m, with solvent signal peak overlap, dppp-ph, $H^{3,8}$-dmp), 7.7 (br, 4H, $H^{5,6}$-dmp), 8.0 (br, 4H, $H^{4,7}$-dmp) ppm. ^{31}P NMR (243 MHz, DMSO): δ = −4.017 (d, J_{Ag-P} = 287 Hz), −4.52 (d, J_{Ag-P} = 248 Hz).

2.2.4. Synthesis of $\{[Ag_2(dppp)_2(Bphen)_2](CF_3SO_3)_2\}_n$ (**4**)

Follow a similar procedure as **2**, dppp (0.2 mmol, 0.0825 g) and Bphen (0.2 mmol, 0.0665 g) were added into the stirring solution of AgOTf (0.2 mmol, 0.0514 g) in a mixture of CH_2Cl_2 (5 ml) and CH_3OH (5 ml) for 5 h at ambient temperature. The insoluble residues were removed by filtration, and the brown filtrate was evaporated slowly at room temperature for about one week to yield white crystals. Yields: 66%. *Anal.* Calc. for $C_{104}H_{84}Ag_2F_6N_4O_6P_4S_2$: elemental analysis: C, 62.34; H, 4.20; N, 2.80%. Measured value:

C, 62.59; H, 4.27; N, 2.76%. IR (cm^{-1}, KBr pellets): 3414s, 3054s, 2426w, 1637s, 1617s, 1588vs, 1560s, 1517s, 1490s, 1435vs, 1384vs, 1335m, 1274vs, 1223s, 1151vs, 1100s, 1029vs, 998m, 956m, 855s, 827m, 766s, 740vs, 723vs, 697vs, 637vs, 593vs, 572s, 546m, 517m, 482s, 444s, 414w. ^{1}H NMR (600 MHz, $CDCl_3$, 298 K): δ = 1.6–2.6 (m, 12H, dppp-$CH_2CH_2CH_2$), 7.0–7.5 (m, with solvent signal peak overlap, dppp-ph, Bphen-ph), 7.5–7.7 (m, 4H, $H^{5,6}$-Bphen), 8.9 (br, 4H, $H^{2,9}$-Bphen) ppm. ^{31}P NMR (243 MHz, $CDCl_3$): δ = 4.68 (d, J_{Ag-P} = 438 Hz), −5.97 (d, J_{Ag-P} = 242 Hz).

2.2.5. Synthesis of {[Ag_2(dppp)$_2$(Bphen)$_2$](ClO$_4$)}$_n$ (**5**)

Follow a similar procedure as **2**, dppp (0.2 mmol, 0.0825 g) and Bphen (0.2 mmol, 0.0665 g) were added into the stirring solution of $AgClO_4$ (0.2 mmol, 0.0415 g) in a mixture of CH_2Cl_2 (5 ml) and CH_3-OH (5 ml) for 5 h at ambient temperature. The insoluble residues were removed by filtration, and the brown filtrate was evaporated slowly at room temperature for about one week to yield white crystals. Yields: 77%. *Anal.* Calc. for $C_{102}H_{84}Ag_2Cl_2N_4O_8P_4$: elemental analysis: C, 64.32; H, 4.41; N, 2.94%. Measured value: C, 64.76; H, 4.52; N, 2.91%. IR (cm^{-1}, KBr pellets): 3435m, 3051m, 2928w, 1965w, 1619m, 1588m, 1560s, 1517s, 1491s, 1434vs, 1424s, 1384s, 1308m, 1270w, 1233m, 1182m, 1097vs, 1026m, 999m, 954m, 854s, 829s, 767vs, 737vs, 701vs, 623vs, 593m, 574m, 547m, 509s, 479s, 441m. ^{1}H NMR (600 MHz, $CDCl_3$, 298 K): δ = 1.5 (br, 4H, dppp-$CH_2CH_2CH_2$), 2.7 (br, 8H, dppp-$CH_2CH_2CH_2$), 7.0–7.6 (m, with solvent signal peak overlap, dppp-ph, Bphen-ph), 7.7 (br, 4H, $H^{5,6}$-Bphen), 8.9 (br, 4H, $H^{2,9}$-Bphen)ppm. ^{31}P NMR (243 MHz, $CDCl_3$): δ = 4.79 (d, J_{Ag-P} = 430 Hz), −5.93 (d, J_{Ag-P} = 233 Hz).

2.3. X-ray crystallographic study of complexes

Single crystals of the complexes were mounted on a Bruker Smart 1000 CCD diffractometer equipped with a graphite-monochromated Mo Kα (λ = 0.71073 Å) radiation at 298 K by ω scanning to collect independent diffraction point. The data is restored by using BRUKER SAINT. All the structures were solved by direct methods using SHELXS program of the SHELXL-97 or SHELXS-97 package and refined with SHELXL-97. Metal atom centers were located from the E-maps and other non-hydrogen atoms were located in successive difference Fourier syntheses. The final refinements were performed by full matrix least-squares methods with anisotropic thermal parameters for non-hydrogen atoms on F2. The hydrogen atoms were generated geometrically and refined with displacement parameters riding on the concerned atoms. Crystallographic data and experimental details for structural analysis are summarized in Table 1. The selected bond lengths and angles, and hydrogen bond lengths and angles of **1**–**5** are given in Table 2.

2.4. Minimum inhibitory concentration (MIC)

Gram-negative bacteria: *E. coli* (ATCC 35210); and Gram-positive bacteria: *S. aureus* (ATCC 25923), *B. subtilis* (ATCC 14593) were used. Sterile nutrient agar (beef extract peptone) plates were prepared by pouring the sterile agar into sterile petri dishes under aseptic conditions and the test organism (0.2 ml) was spread on the plates. Holes (5 mm diameter) were made in the agar plates by use of a sterile bore. Test complexes, standard drug, and the DMSO (as control) were placed in separate holes. The plates were maintained at +4 °C for 1 h to enable diffusion of the solutions into the agar medium. Plates containing bacteria were incubated at 37 °C for 24 h. The changes of inhibition zones of complexes **1**–**4** are shown in Figs. S1 and S2. After quantitative determination, the qualitative analysis was conducted. The MIC values of all the complexes were also determined, by use of the broth-dilution method. A series of test tubes were prepared containing the same volume of medium inoculated with the test organism (the inoculum may vary from 10^5 to 10^6 cells per milliliter). Decreasing concentrations of the test complexes were added to the tubes; stepwise dilution by a factor of 2 (twofold serial dilution) was usually used (80 μg/ml, 40 μg/ml, 20 μg/ml, etc.) [30–33]. One tube was left without test complexes, to serve as a positive control for growth of the organism. The cultures were incubated. The tubes were inspected visually to monitor growth of the organism (indicated by turbidity); tubes containing the antimicrobial agent at a concentration sufficient to inhibit growth remained clear. Experimentally, the MIC is the concentration of the test complexes

Table 1
Crystallographic data for complexes **1**–**5**.

Complex	**1**	**2**	**3**	**4**	**5**
Formula	$C_{78}H_{72}Ag_2B_2F_8N_4O_2P_4$	$C_{84}H_{76}Ag_2F_6N_4O_6P_4S_2$	$C_{83}H_{80}Ag_2B_2F_8N_4OP_4$	$C_{104}H_{84}Ag_2F_6N_4O_6P_4S_2$	$C_{102}H_{84}Ag_2Cl_2N_4O_8P_4$
Mr	1610.63	1755.22	1662.75	2003.49	1904.25
Temperature (K)	298(2)	298(2)	298(2)	298(2)	298(2)
Crystal system	triclinic	triclinic	triclinic	monoclinic	monoclinic
Space group	$P\bar{1}$	$P\bar{1}$	$P\bar{1}$	*P*2(1)/*c*	*P*2(1)/*c*
a (Å)	12.9107(11)	11.3210(9)	11.3410(9)	13.1670(11)	12.1338(11)
b (Å)	13.0306(12)	13.3819(11)	13.6059(12)	32.260(3)	28.850(2)
c (Å)	13.6106(13)	14.0121(13)	13.6461(12)	23.7200(19)	14.0899(12)
α (°)	113.442(2)	75.3680(10)	104.684(2)	90.00	90.00
β (°)	94.5040(10)	79.180(2)	92.6160(10)	91.1720(10)	110.776(3)
γ (°)	112.875(2)	89.145(3)	99.4490(10)	90.00	90.00
V(Å^3)	1860.5(3)	2016.2(3)	2000.8(3)	10073.4(14)	4611.6(7)
Z	1	1	1	4	2
D_{calc} (Mg/m^3)	1.438	1.446	1.380	1.321	1.371
θ (°)	25.02	25.02	25.02	25.02	25.02
F(000)	820	896	850	4096	1952
Data/restraint/parameters	6469/0/468	6990/0/514	6900/0/497	17742/0/1191	8132/0/587
Reflections collected	9352	10259	10050	50992	18444
Goodness-of-fit on F^2	1.051	1.031	1.073	1.067	1.041
R_{int}	0.0277	0.0221	0.0267	0.0716	0.1006
$R_1[I > 2\sigma(I)]$	0.0492	0.0525	0.0516	0.0925	0.0772
wR_2 [I>2σ(I)]	0.1249	0.1243	0.1333	0.2147	0.1581
R_1 (all data)	0.0765	0.0846	0.0827	0.1877	0.1674
wR_2 (all data)	0.1547	0.1430	0.1522	0.2297	0.2089
Residuals (e Å^{-3})	0.672, −0.858	0.655, −0.455	0.759, −0.449	1.170, −0.522	0.960, −0.595

Table 2
Selected bond lengths (Å) and angles (°) for complexes **1**–**5**.

Bond length (Å)		Bond angle (°)	
Complex ***1***			
Ag(1)–P(1)	2.438(2)	P(1)–Ag(1)–P(2)	132.29(6)
Ag(1)–P(2)	2.453(5)	P(1)–Ag(1)–N(1)	114.40(4)
Ag(1)–N(1)	2.390(4)	P(1)–Ag(1)–N(2)	103.73(4)
Ag(1)–N(2)	2.422(7)	P(2)–Ag(1)–N(1)	105.66(6)
		P(2)–Ag(1)–N(2)	113.91(9)
		N(1)–Ag(1)–N(2)	69.77(8)
Complex ***2***			
Ag(1)–P(2)	2.449(4)	P(1)–Ag(1)–P(2)	140.13(5)
Ag(1)–P(1)	2.400(2)	P(1)–Ag(1)–N(1)	115.27(2)
Ag(1)–N(1)	2.402(8)	P(1)–Ag(1)–N(2)	116.25(2)
Ag(1)–N(2)	2.412(6)	P(2)–Ag(1)–N(1)	94.34(7)
		P(2)–Ag(1)–N(2)	98.22(8)
		N(1)–Ag(1)–N(2)	69.81(8)
Complex ***3***			
Ag(1)–N(1)	2.399(7)	N(1)–Ag(1)–P(2)	115.43(3)
Ag(1)–N(2)	2.404(6)	N(1)–Ag(1)–P(1)	99.02(7)
Ag(1)–P(1)	2.455(3)	P(2)–Ag(1)–P(1)	139.37 (5)
Ag(1)–P(2)	2.405(2)	N(1)–Ag(1)–N(2)	70.68(8)
		P(2)–Ag(1)–N(2)	116.46(7)
		P(1)–Ag(1)–N(2)	94.15(4)
Complex ***4***			
Ag(1)–N(1)	2.468(6)	N(1)–Ag(1)–N(2)	67.62(5)
Ag(1)–N(2)	2.421(7)	N(1)–Ag(1)–P(1)	96.91(6)
Ag(1)–P(1)	2.439(6)	N(2)–Ag(1)–P(1)	98.82(9)
Ag(1)–P(2)	2.416(4)	N(1)–Ag(1)–P(2)	106.83(6)
Ag(2)–N(3)	2.486(8)	N(2)–Ag(1)–P(2)	104.09(8)
Ag(2)–N(4)	2.415(7)	P(1)–Ag(1)–P(2)	151.80(8)
Ag(2)–P(3)	2.446(6)	P(3)–Ag(2)–P(4)	148.25(8)
Ag(2)–P(4)	2.430(4)	N(3)–Ag(2)–P(3)	95.78(9)
		N(3)–Ag(2)–P(4)	106.80(7)
		N(4)–Ag(2)–P(3)	104.50(8)
		N(4)–Ag(2)–P(4)	104.66(6)
		N(3)–Ag(2)–N(4)	67.30(2)
Complex ***5***			
Ag(1)–N(1)	2.393(8)	N(2)–Ag(1)–P(1)	106.83(5)
Ag(1)–N(2)	2.451(7)	N(1)–Ag(1)–P(1)	118. 32(5)
Ag(1)–P(1)	2.390(4)	P(1)–Ag(1)–P(2)	142.65 (8)
Ag(1)–P(2)	2.440(6)	N(1)–Ag(1)–P(2)	97.53(9)
		N(2)–Ag(1)–P(2)	95.36 (7)
		N(2)–Ag(1)–N(1)	68.35(3)

present in the last clear tube, i.e. the tube containing the lowest concentration of test complexes in which growth is not observed. The synthesized complexes were checked, in vitro, for inhibitory activity against three microorganisms—the bacteria *S. aureus*, *B. subtilis*, *E. coli*. Penbritin was used as controls. In addition, the antimicrobial activity of the "free" ligands (dppp, Bphen, dmp, phen) was examined using the same method, showing that it is inactive at the maximum concentration.

3. Results and discussion

3.1. Synthesis of complexes *1*–*5*

Five complexes **1**–**5** were synthesized by the reactions of silver (I) salt with dppp, 1,10-phenanthroline and its derivative in the mixture solvent of dichloromethane and methanol (Scheme 1). Each asymmetry unit of these five complexes is a dinuclear molecule. In complexes **1**–**4** topologically promising architectures are further formed through hydrogen bonds between the C–H groups of aromatic ring and anions. This is because the F atom from trifluoromethanesulfonate anions ($CF_3SO_3^-$) or tetrafluoroborate anions (BF_4^-) in **1**–**4** has stronger electronegativity than the O atom from perchlorate anions (ClO_4^-) in **5**, the intermolecular hydrogen bonds (C–H···F) between the C–H group of benzene ring and the F atom

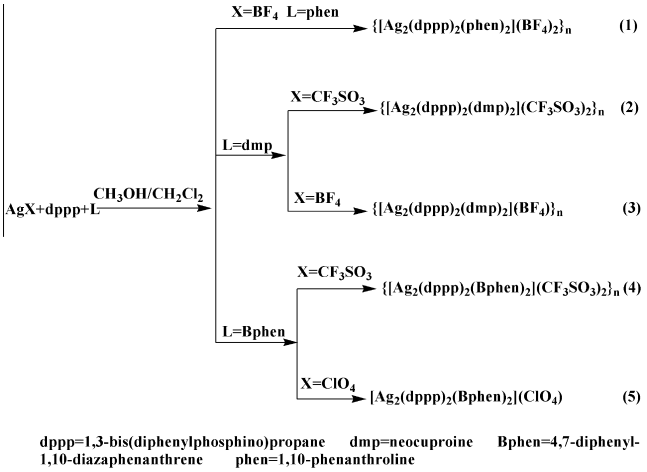

Scheme 1. The routine of synthesis for complexes **1**–**5**.

from the anion can be formed in **1**–**4** to generate 3D supramolecular structure. The complexes **1**–**4** have different topologically architectures, due to the different anions and different N-donor ligands in them.

3.2. Single crystal X-ray studies

3.2.1. Complex $\{[Ag_2(dppp)_2(phen)_2](BF_4)_2\}_n$ (*1*)

The coordination geometry of the Ag atom of **1** was best described as distorted tetrahedron with each Ag atom coordinated to two phen-nitrogen atoms and two P atoms from dppp ligands (Fig. 1). The two N_2Ag^+ fragments are bridged by two dppp ligands to form a twelve-membered ring. The average Ag–N and Ag–P distances are 2.406 Å and 2.446 Å, respectively, which are longer than those of $[Ag_2(phen)_2(\mu\text{-dppp})_2]_2^+$ [8] (Ag–N: 2.397 Å, Ag–P: 2.426 Å). The N–Ag–N angle of 69.8(8)° is comparable to that observed in other silver(I) complexes [70.2(7)°] containing phen ligand [8], whereas the P–Ag–P angle of 132.3(6)° is slightly smaller than that of $[Ag(dppp)(phen)](ClO_4)$ [30] (P–Ag–P: 145.49(3)°). To understand the structure of complex **1**, a topology analysis is employed to describe the architecture. Every $Ag_2P_4C_6$ ring is linked by C–H···F hydrogen bonds between the C–H groups of aromatic ring and fluorine atoms from BF_4^-, which results in a 2-D infinite network. The architecture of complex **1** can be reduced to a topology structure by considering the $Ag_2P_4C_6$ ring as a six-connected node which connect four similar rhomboids and two four-membered rings (Fig. 1a).

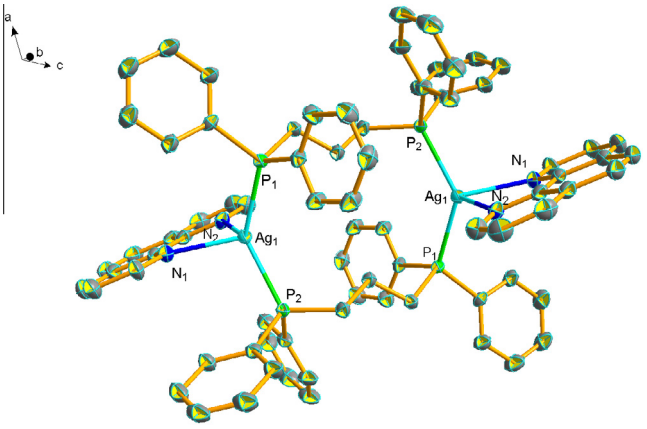

Fig. 1. The molecular entities of complex **1** (The H atoms and H_2O molecular are omitted for clarity). Thermal ellipsoids drawn at the 30% probability level.

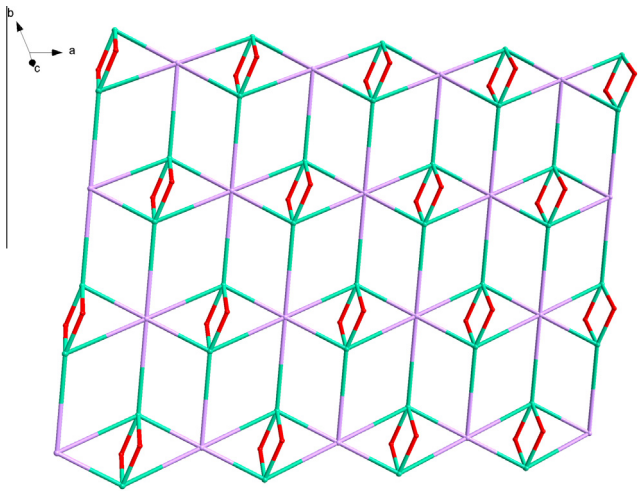

Fig. 1a. The 2-D structure bridging by hydrogen bonds of complex **1**.

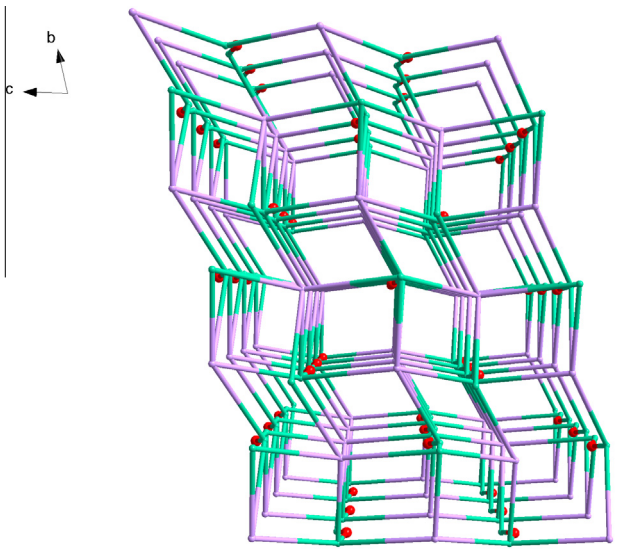

Fig. 2a. The 3-D structures bridging by hydrogen bonds of **2** along the a axis.

*3.2.2. Single crystal structure analysis of complexes {[Ag_2(dppp)$_2$(dmp)$_2$][CF_3SO_3)$_2$}$_n$ (**2**) and {[Ag_2(dppp)$_2$(dmp)$_2$][BF_4)}$_n$ (**3**)*

In complexes **2** and **3**, two distorted tetrahedron silver(I) centers are wrapped around by two dmp molecules and two dppp ligands (Figs. 2 and 3), and N_2Ag^+ fragments are bridged by two bulky dppp ligands forming a $Ag_2P_4C_6$ ring, which is similar to complex **1**. Complexes **2** and **3** are also of dinuclear structures. In complex **2**, every Ag(1) atom is coordinated by two nitrogen atoms of one dmp molecule with the mean Ag–N distance of 2.407 Å and two phosphorus atoms from two dppp molecules with the mean Ag–P distance of 2.425 Å. The angles of P(2)–Ag(1)–P(1) and N(2)–Ag(1)–N(1) are 140.1(5)° and 69.8(8)°, respectively, which are similar to [Ag(dppp)(dmp)](ClO_4) [34] (P(2)–Ag(1)–P(1):139.2(1)°, N(2)–Ag(1)–N(1):70.8(5)°). The bond lengths of Ag–N (2.407 Å) and Ag–P (2.425 Å) of complex **2** are similar to the bond lengths of Ag–N (2.399 Å) and Ag–P (2.455 Å) of complex **3**, and they are longer than the bond lengths of Ag–N (2.388(1) Å) and Ag–P (2.391(4) Å) of the complex [Ag(dppp)(dmp)](ClO_4) [34]. Compared with complex **1**, complexes **2** and **3** have more complicated 3D topologies. The single-crystal X-ray diffraction reveals that complexes **2** and **3** crystallize in triclinic system with the space group $P\bar{1}$, exhibiting the three-dimensional framework consisting of dinuclear structures of [$Ag_2P_4C_6$] ring, linked by C–H···F hydrogen bonds (Figs. 2a, S3, S4, 3a, S5 and S6).

*3.2.3. Single crystal structure analysis of complexes {[Ag_2(dppp)$_2$(Bphen)$_2$][CF_3SO_3)$_2$}$_n$ (**4**) and [Ag_2(dppp)$_2$(Bphen)$_2$][ClO_4) (**5**)*

Complexes **4** and **5** have similar molecular structures. In complexes **4** and **5**, two P atoms from two different dppp ligands and two N atoms from one Bphen molecule are coordinated to the Ag(I) atom, forming a distorted tetrahedron configuration. In complexes **4** and **5**, the dppp ligand adopts bridging coordination mode and 1,10-phenanthroline derivative adopts chelating coordination mode to form the dinuclear structures (Figs. 4 and 5). In addition, trifluoromethanesulfonate anion ($CF_3SO_3^-$) and perchlorate anion (ClO_4^-) are uncoordinated in complexes **4** and **5**. It is noteworthy that in the complex **4**, there are two different Ag(I) centers resulting to two dinuclear units (Fig. 4a). The angle of two center $Ag_2P_4C_6$ rings from two different dinuclear units is 50. 3(7)°. In complex **4**, the average bond lengths of Ag1–P, Ag1–N, Ag2–P and Ag2–N are 2.428 Å, 2.445 Å, 2.438 Å and 2.451 Å, respectively, which are longer than those in complex $[Ag_2(Bphen)_2(\mu\text{-dppm})]_2^+$ (Ag1–N (2.30 Å), Ag2–N (2.310 Å), Ag1–P (2.357(3) Å), Ag2–P

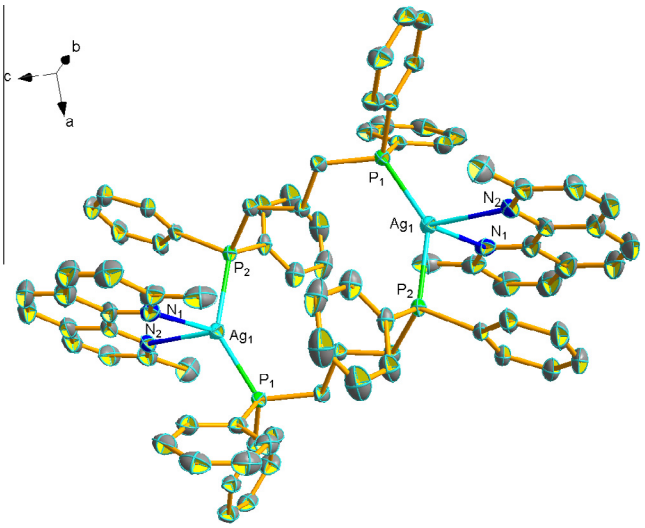

Fig. 2. The molecular entities of complex **2** (The H atoms are omitted for clarity). Thermal ellipsoids drawn at the 30% probability level.

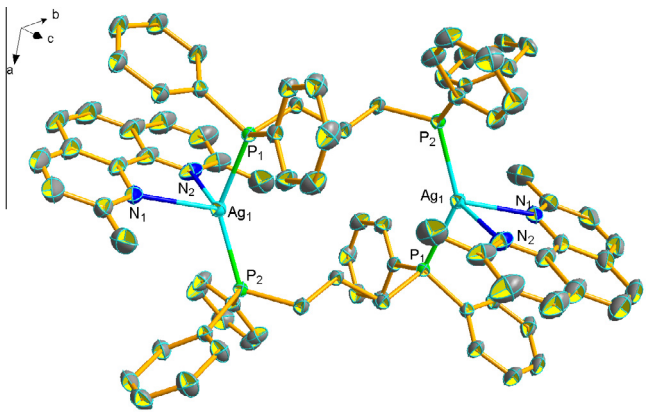

Fig. 3. The molecular entities of complex **3** (The H atoms are omitted for clarity). Thermal ellipsoids drawn at the 30% probability level.

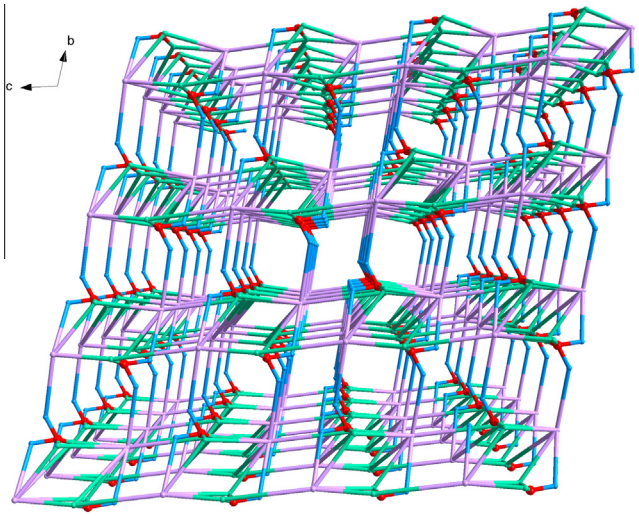

Fig. 3a. The 3-D structures bridging by hydrogen bonds of **3** along the a axis.

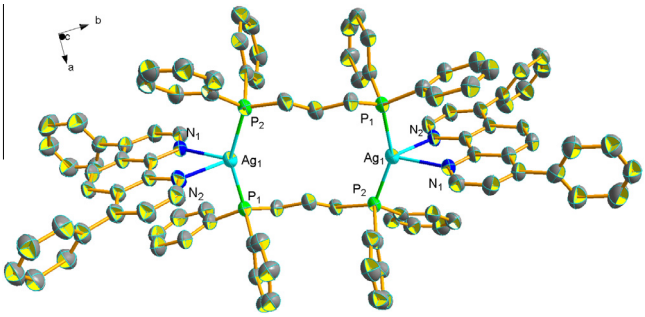

Fig. 4. The molecular entities of complex **4** (the H atoms are omitted for clarity). Thermal ellipsoids drawn at the 30% probability level.

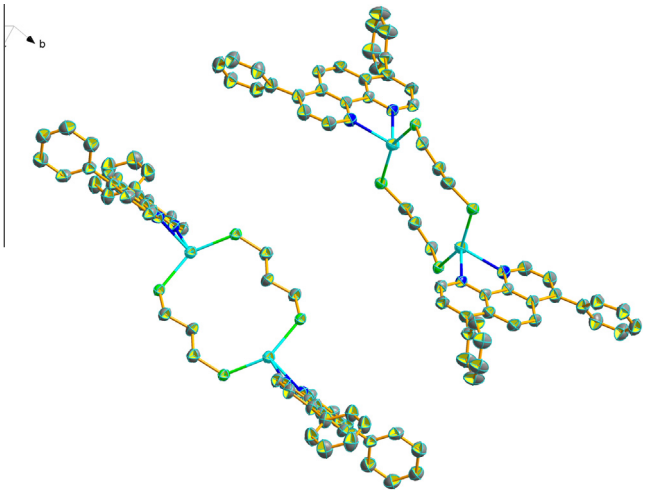

Fig. 4a. Two different dinuclear structures with a torsion angle.

(2.357(3) Å)) [8]. The angles of P–Ag1–N, P–Ag2–N are in the fluctuation range of [96.9(2)–106.8(2)°], [95.8(9)–106.8(7)°], respectively, which is bigger than the complex $[Ag_2(Bphen)_2(\mu\text{-dppm})]^{+}_{2}$ [8] (P–Ag1–N:141.1(3)–146.3(3)°, P–Ag2–N: 139.4(2)–147.6(3)°). In complex **4**, trifluoromethanesulfonate anion ($CF_3SO_3^-$) doesn't participate in coordination. The F atom and O atom from trifluoromethanesulfonate anion ($CF_3SO_3^-$) are modeled as disordered around two positions in ratio 0.36:0.64. In complex **5**, there exists only one Ag(I) center, which is different from the complex **4**. In complex **5**, the average bond lengths of Ag–P [2.415 Å], Ag–N [2.422 Å] are slightly shorter than those of complex **4** [Ag1–P: 2.428 Å, Ag1–N: 2.450 Å, Ag2–P: 2.438 Å and Ag2–N: 2.451 Å]. The fluctuation range of angle of P–Ag–N is 95.4(7)–118.3(5)°, which is obvious smaller than that of complex **4** [P–Ag1–N: 96.9 (2)–106.8(6)°, P–Ag2–N: 95.7(9)–106.8(7)°]. Thus the distortion degree of the tetrahedral configuration is less than that of complex **4**. From the data of bond lengths and angles, we can see that due to the steric effect of the benzene from Bphen and diphosphine ligands, there exists an unfavorable repulsion between the Ag(I) center and diphosphine ligands which makes a distorted tetrahedron configuration of **4**. The single-crystal X-ray diffraction reveals that complexes **4** and **5** crystallize in the monoclinic system with the space group P2(1)/c, but only complex **4** exhibits a three-dimensional framework, linked by C–H···F hydrogen bonds (Fig. 4b). To best understand the structure of complex **4**, a topology analysis is employed to describe the architecture. It is interesting that two adjacent Ag(I) atoms are linked by two dppp molecules to generate a dinuclear structure. The dinuclear structure of complex **4** is further linked into a 3-D supramolecular structure through C–H···F hydrogen bonds between the C–H groups of aromatic ring and fluorine atoms from trifluoromethanesulfonate anion ($CF_3SO_3^-$). The architecture of complex **4** can be reduced to a nodal topology structure by considering F atom as a four-connected node (Fig. 4c–e). Compared with the structure of complex **4**, the structure of complex **5** is simple, it is a dinuclear structure consisting of $[AgN_2P_2]$ tetrahedron. This is because the F atom from trifluoromethanesulfonate anion ($CF_3SO_3^-$) has a larger electronegativity than the O atom from perchlorate (ClO_4^-).

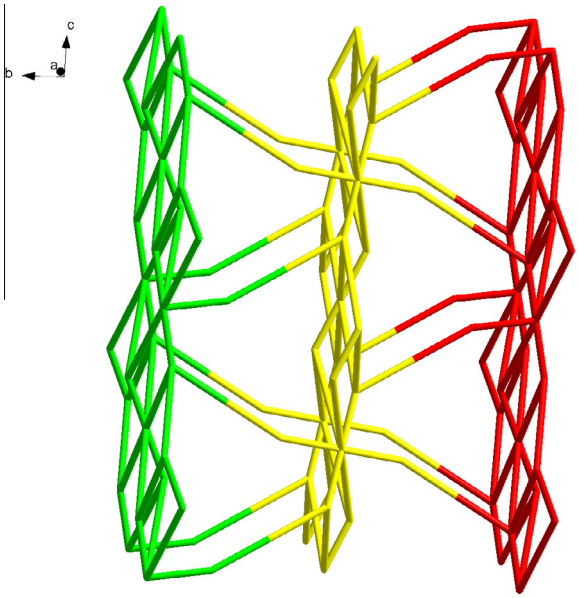

Fig. 4b. The 3-D structures bridging by hydrogen bonds of complex **4**.

4. Spectroscopy properties analysis

4.1. Luminescent properties

At ambient temperature, the luminescent excitation and emission spectra of complexes **1**–**5** and reacting material are measured in solid state (Fig. 6). The 1,10-phenanthroline derivatives exhibit luminescent signal centered at 420 nm (λ_{ex} = 351 nm for phen),

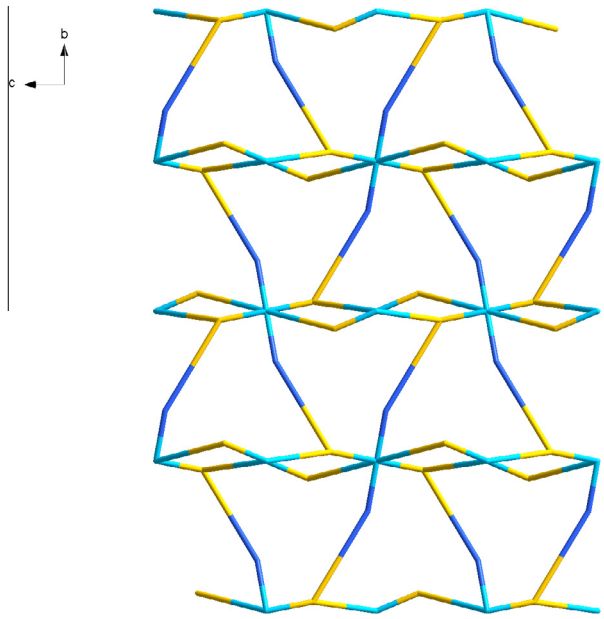

Fig. 4c. The 3-D structures bridging by hydrogen bonds of **4** along the a axis.

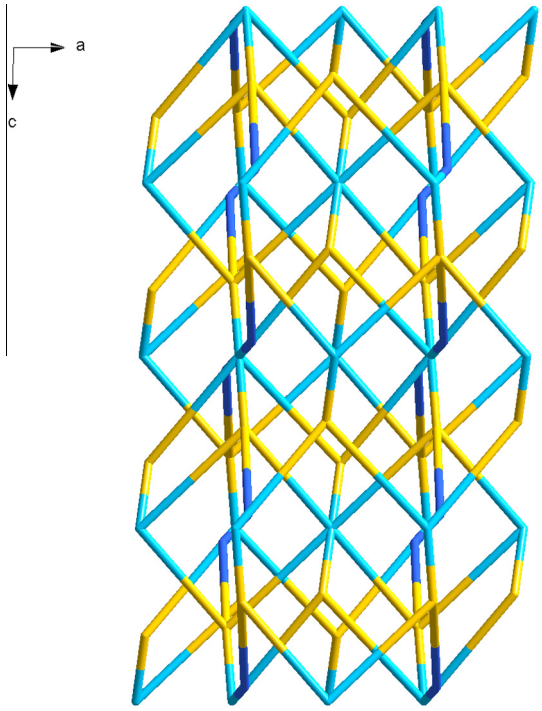

Fig. 4d. The 3-D structures bridging by hydrogen bonds of **4** along the b axis.

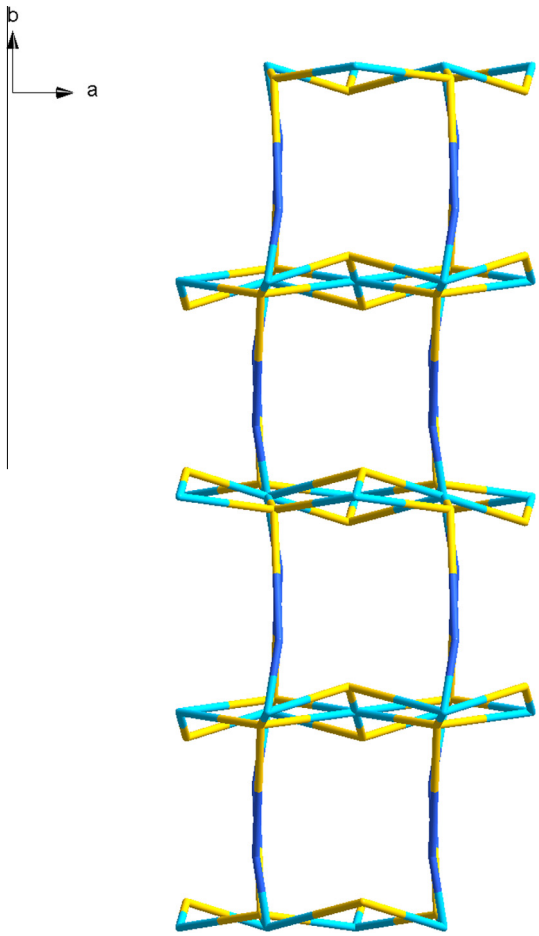

Fig. 4e. The 3-D structures bridging by hydrogen bonds of **4** along the c axis.

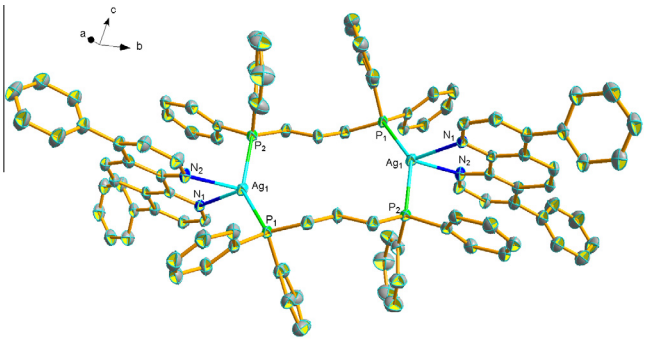

Fig. 5. The molecular entities of complex **5** (the H atoms are omitted for clarity). Thermal ellipsoids drawn at the 30% probability level.

422 nm (λ_{ex} = 347 nm for dmp), 422 nm (λ_{ex} = 353 nm for Bphen). Dppp is excited at the excitation wavelength of 356 nm, finding that the emission maximum is exhibited at 424 nm. In the emission spectra of complexes **1**–**3**, the emission peaks are found at 443 nm (λ_{ex} = 367 nm for **1**), 423 nm (λ_{ex} = 363 nm for **2**), 447 nm (λ_{ex} = 378 nm for **3**), respectively. The peaks in 420–440 nm are assigned to the intraligand emissions derived from ligand-centered [π–π*] transition. Compared with the free diphosphine ligands, all the excited spectral and the emission spectral peaks of these complexes move toward long-wave and exhibit red-shifted. The complex **5** has two emission spectral peaks. The emission spectral peaks at 557 nm (λ_{ex} = 345 nm) in complex **5** and at 505 nm (λ_{ex} = 407 nm) in complex **4** are assigned to MLCT/LMCT [35–37] which is caused by Ag–N containing chromophores. The emission spectral peak of complex **5** at 422 nm (λ_{ex} = 345 nm) is attributed to π–π* transition of the two ligands.

4.2. ^{1}H NMR and ^{31}P NMR

At room temperature, the ^{1}H NMR and ^{31}P NMR spectra have been measured in $CDCl_3$ solution (for **1**, **2**, **4**, **5**) and in DMSO solution (for **3**). The ^{1}H NMR spectra exhibit the signal of the protons of C–H adjacent to the N atom from 1,10-phenanthroline derivatives

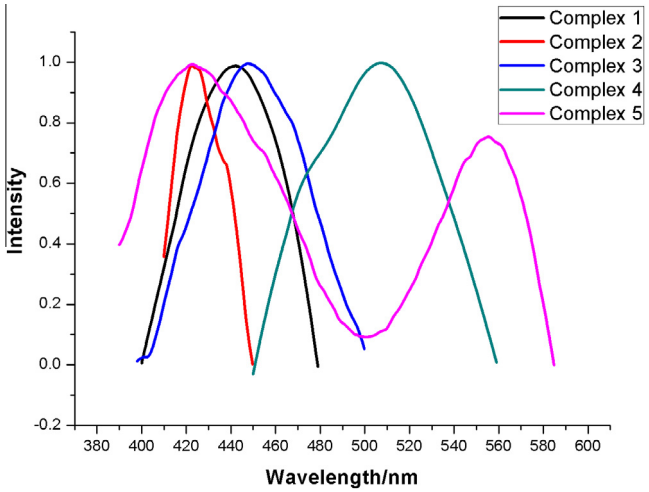

Fig. 6. The luminescent emission spectra of complexes **1**–**5** in the solid state at room temperature.

at 8.2–8.9 (broad peak) ppm(for complexes **1**, **4**, **5**) and 7.9–8.1 (multiplet peak) ppm(for complexes **2**, **3**). The multiple signals in the range of 7.6–7.7 ppm are assigned to the other protons from 1,10-phenanthroline derivatives. The multiple resonance signals in the range of 7.2–7.5 ppm are assigned to protons from benzene ring of diphosphine ligands. In complexes **2**, **4**, **5**, the signals of methylene of dppp are in the range 1.5–1.6 ppm (multiplet peaks) and 2.3–2.7 ppm (multiplet peaks), which indicate that the environment of dppp in the complexes are similar. In complex **1**, there are multiplet peaks in the range of 1.2–1.5 ppm, which is attributed to protons of three methylenes from dppp. In complex **3**, the broad signals centered at 3.3 ppm is assigned to protons of two methylenes connecting with two P atoms of dppp, and the broad signals centered at 2.4 ppm is ascribed to the protons of the other methylene of dppp.

In ^{31}P NMR spectra of **1**–**5**, the two phosphorus atoms in each molecule are found to have different resonance signals. The similarity of resonance signals in solution of **1**, **4**, **5** show that the chemistry environment for the phosphorus atom from diphosphine ligands is similar. In complexes **1**–**5**, each complex exhibits two peaks because the two phosphorus atoms in each molecule are not chemically equivalent.

4.3. Antibacterial activity

The antimicrobial activity of complexes **1**–**5** and free ligands have been tested in vitro using the serial dilutions method against selected Gram-negative (*E. coli*) and Gram-positive (*B. subtilis*, *S. aureus*) bacteria. The obtained results are presented as minimal inhibitory concentrations (MIC, μg mL^{-1}) in Table 3. The free ligands (dppp, phen, dmp, Bphen) are inactive against the tested bacteria strains. All of the tested complexes exhibit comparable antimicrobial activities against *E. coli* bacteria, *B. subtilis* bacteria and *S. aureus* bacteria with MIC values in the ranges of 2.5–5 μg mL^{-1}, 2.5–10 μg mL^{-1} and 5–10 μg mL^{-1}, respectively. Minimal inhibitory concentrations (MICs) of complexes **1** (2.5–5 μg/ml), **2** (2.5–5 μg/ml), **4** (2.5–5 μg/ml) are overall lower than those obtained for complex **3** (5–10 μg/ml) against both bacteria. The complexes **1**–**4** have a higher activity against the Gram-negative species (*E. coli*, MIC range = 2.5–5 μg/ml) with respect to the Gram-positive ones (*B. subtilis*, MIC range = 2.5–10 μg/ml, *S. aureus*, MIC range = 5–10 μg/ml). There is no antimicrobial activity for complex **5**. It is noteworthy that the antimicrobial activity against the bacteria of complex **4** (2.5–5 μg/ml) is higher than complexes **1**–**3** (2.5–10 μg/ml), which maybe is due to the existence of two different dinuclear units in the crystal lattice of complex **4**. We found that complexes **1**–**4** had better antibacterial activity against *E. coli* bacteria and *S. aureus* bacteria than the complexes in literature [20] (with MIC values in the 6–7 μg mL^{-1} and 6–40 μg mL^{-1} ranges, respectively). On the basis of the above observations, we can know that the difference in the antimicrobial efficiencies of complexes **1**–**5** is mostly related to the different quantity of silver ions per molecule and the type of coordination environment of the silver(I) atom [20,21].

Table 3
Antimicrobial activity of compounds **1**–**4** expressed as minimum inhibitory concentration (MIC μg mL^{-1}).

Strain	MIC (μg mL^{-1})				Normalized MIC (nmol mL^{-1})[a]			
	1	**2**	**3**	**4**	**1**	**2**	**3**	**4**
E. coli	2.5	2.5	5.0	2.5	3.1	2.8	6.0	2.5
B. subtilis	5.0	5.0	10.0	2.5	6.2	5.6	12.0	2.5
S. aureus	5.0	5.0	10.0	5.0	6.2	5.6	12.0	5.0

[a] These MIC values were normalized for the number of silver atoms in each compound.

4.4. The study of THz spectroscopy properties

The room temperature terahertz (THz) absorption spectra of metal salts ($AgClO_4$, $AgBF_4$, $AgCF_3SO_3$), diphosphorus ligands (dppp), 1,10-phenanthroline derivative (phen, dmp, Bphen) and complexes **1**–**5** were measured in the range of 0.2–4.0 THz. All the above complexes have characteristic resonance peaks. The found peaks for each complex are as following: dppp (0.27, 0.37, 0.42, 0.56, 0.66, 1.07, 1.27 and 1.38 THz), phen (1.05, 1.58, 1.76, 2.17, 2.51 and 2.75 THz), dmp (0.76, 1.05, 2.24, 2.58, 2.69 and 2.82 THz), Bphen (0.23, 0.4, 0.53, 0.65, 0.76, 0.94, 1.29, 1.46, 2.30, 2.57, 2.70, 2.81, 2.93, 3.11 and 3.24 THz), $AgClO_4$ (2.46, 2.58, 2.70, 3.04 and 3.16 THz), $AgBF_4$ (0.38, 0.46 and 0.51 THz), $AgCF_3SO_3$ (0.69, 0.84, 1.00, 1.16 and 1.30 THz), complex **1** (0.39, 1.02, 1.45, 2.03, 2.36, 2.58, 2.70, 2.81, 2.94, 3.10 and 3.45 THz), complex **2** (0.50, 1.28, 1.84, 2.33, 2.47, 2.58, 2.69, 2.81, 2.93, 3.22 and 3.35 THz), complex **3** (0.38, 0.88, 1,06, 1.30, 2.04, 2.22, 2.37, 2.47, 2.58, 2.69, 2.81, 2.93, 3.23 and 3.35 THz), complex **4** (0.24, 0.41, 0.54, 0.94, 1.05, 1.17, 1.31, 1.83, 1.94, 2.33, 2.46, 2.59, 2.69, 2.81, 2.93, 3.22 and 3.41 THz), complex **5** (0.41, 0.75, 0.94, 1.30, 1.62, 2.09, 2.46, 2.58, 2.69, 2.81, 2.93, 3.20 and 3.35 THz). Although the agreement between crystal structure and observed spectra does not allow a definitive characterization, it is possible to make tentative assignments of many observed features in the terahertz region for the samples [38]. By comparing the THz absorption spectra of the products with those of the reactants, we can see that most peaks of the diphosphorus ligands and AgX disappear or move, and new peaks in the range of 2.81–3.45 THz appear in the obtained complexes. The founded peaks for five complexes are shown in Fig. 7. We can see that the whole peaks of complexes **1**–**5** are nearly the same, which shows that THz-TDS may be an effective method to determine the difference of isostructural metal–ligand complexes [39,40]. Complexes **1** and **3** have the same space groups, but are of different topological configuration. The weak and small peaks in complex **1** are due to the strong rigidity of phen ligand in complex **1**. The THz absorption peaks before 2.2 THz in the spectrum of complex **2** exhibits blue-shifted compared with complex **3**, which indicate that the difference of anions has impact on skeleton vibration of configuration of complexes. In previous studies, we also have found that the coordination of inorganic anions have influence on THz absorption spectra of complexes of 1D configuration [41]. By comparing the THz

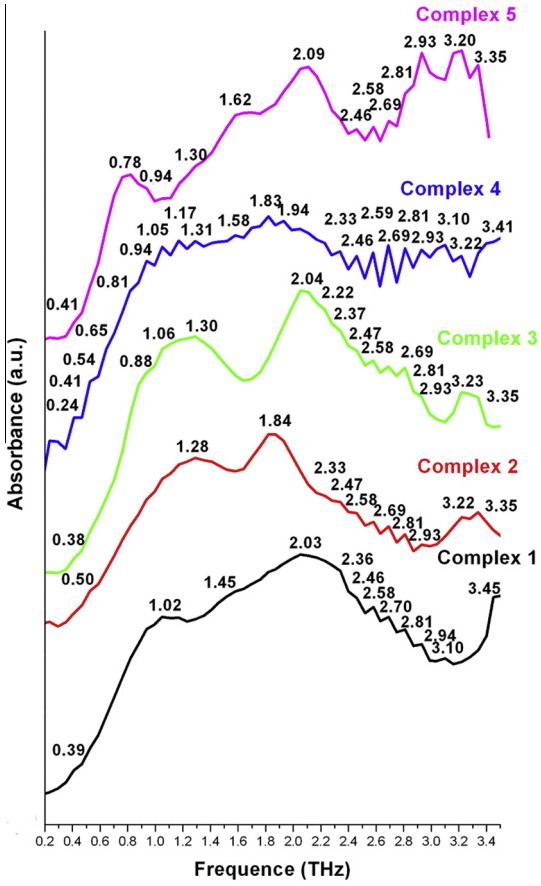

Fig. 7. The terahertz spectrum of complexes **1**–**5** in the range of 0.2–4.0 THz.

absorption spectra of complexes **2** and **4**, we see that the complex **4** has smaller and weaker peaks, which is due to the fact that the strength of skeleton vibration of Bphen ligand in complex **4** is weaker than that of dmp ligand in complex **2**. Compared with complex **4**, the strength of the THz absorption peaks of complex **5** is stronger, showing strength of skeleton vibration of binuclear structure in **5** is stronger than that of 3D configuration in **4**. The discovery is a supplement for THz spectroscopy properties of Ag complexes containing nitrogen and phosphorous ligands [42]. THz-TDS provides many characteristic peaks to these new complexes. It may be a sensitive method to further determine some of the inorganic–organic hybrid complexes, especially those isostructural complexes which are difficult to be identified by other spectroscopy [42,43].

4.5. Thermogravimetric analysis

In order to investigate the thermal stability of these complexes, TGA analyses are carried out for complexes **1**–**5**. Experiments of these samples were carried out from room temperature to 800 °C. It was found that the TGA curves of complex **1** showed one-step weight loss profile, while the TGA curves of **2**–**5** showed two-step weight loss processes (Fig. 8).

It is amazing that the complexes **1**–**5** possess good thermal stability up to 350 °C due to the existence of dppp and 1, 10-phenanthroline derivatives in the complexes. Some caution should be taken that complexes containing perchlorate anion are unstable, they can decompose even explode easily under low temperature. But complex **5** can still be measured by thermogravimetric analysis and it shows good thermal stability. The complexes **2**–**4** have better thermostability overtoping 400 °C than the complexes **1** and **5** due to their 3D network structures. The complex **4** has best thermostability, which maybe is due to the existence of two binuclear structural units with a torsion angle formed through two different Ag(I) centers in the crystal lattice of complex **4**. In the temperature range of 350–650 °C, complexes **2** and **3** rapidly decompose to silver oxides, while the complexes **1**, **4** and **5** rapidly decompose to elemental silver.

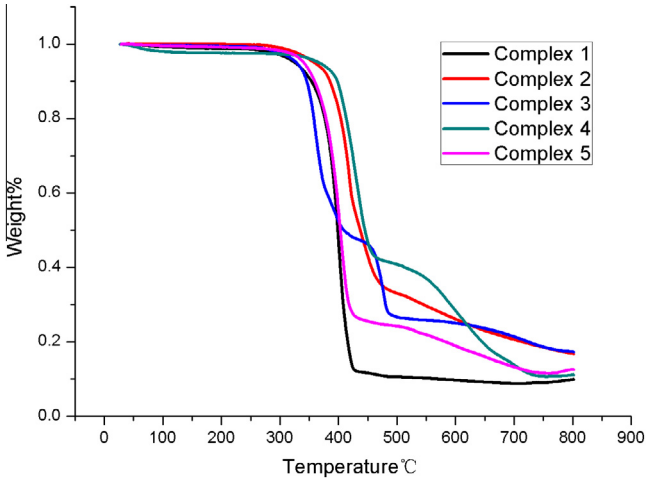

Fig. 8. Thermogravimetric analysis (TGA) curves for the heating of complexes **1**–**5** to 800 °C in dry air.

In complexes **1**–**5**, the initial weight loss in the temperature range 100–350 °C is assigned to the removal of solvent attaching to the surface of crystal per formula unit. When the temperature is up to 350 °C, these complexes began to decompose rapidly. In complexes **1**–**5**, the final weight loss of 86.8% (calcd 86.4%) for **1**, 84.1% (calcd 86.8%) for **2**, 83.6% (calcd 86.1%) for **3**, 88.9% (calcd 89.2%) for **4**, 87.5% (calcd 88.7%) for **5** in the temperature range 350–800 °C is assigned to the removal of ligands per formula unit.

5. Conclusion

Five new Ag(I) complexes containing 1,10-phenanthroline derivative and dppp have been synthesized and characterized by IR, elemental analysis, luminescence, NMR spectroscopy, antibacterial activity, THz time domain spectroscopy and thermogravimetric analysis. Five Ag(I)-dppp complexes with 1,10-phenanthroline derivative are synthesized by one-step way and characterized by X-ray single crystal structure for the first time. Five complexes are all of dinuclear structures and complexes **1**–**4** have topologically promising architectures generated through hydrogen bonds (F···H–C) between the C–H groups of aromatic ring and anions. Complexes **1**–**5** exhibit interesting fluorescence emission spectrum in the solid state. Compared with the free ligands, the emission spectra of all these complexes exhibit red-shifted. The complex **5** has two emission spectral peaks. The emission spectral peak at 557 nm (λ_{ex} = 345 nm for **5**) is assigned to MLCT/LMCT which is caused by Ag–N containing chromophores and the emission spectral peak of complex **5** at 422 nm (λ_{ex} = 345 nm for **5**) is attributed to π–π^* transition of ligands. The flexible phosphine ligands, inorganic anions, the metal–ligand coordination and hydrogen bond can affect the THz spectra of Ag(I) complexes. The hydrogen bonds formed by inorganic anions ($CF_3SO_3^-$, BF_4^-, ClO_4^-) leading to different steric configuration have significant influence on THz absorption spectroscopy. Moreover, this series of studies further enrich the THz spectroscopy properties of Ag complexes with nitrogen and phosphorous ligands, and

may help to lay the foundation for the identification of THz time domain spectroscopy. Complexes **1**–**4** exhibit significant antibacterial activity, they may be further explored as potential novel bioactive materials.

Acknowledgements

This work has been supported by the National Natural Science Foundation of China (Grant No. 21171119, 11104360 and 11204191), the National High Technology Research and Development Program 863 of China (Grant No. 2012AA063201) and the Committee of Education of the Beijing Foundation of China (Grant No. KM201210028020), Scientific Research Base Development Program of the Beijing Municipal Commission of Education, the National Special Fund for the development of Major Research Equipment and Instruments (Grant No. 2012YQ14000508) and Technology Foundation for Selected Overseas Chinese. The Beijing Municipal Education Commission (KM201510028006) and the Scientific Research Base Development Program of the Beijing Municipal Commission of Education.

Appendix A. Supplementary data

CCDC 1408310, 1408311, 1408312, 1408313 and 1408314 contains the supplementary crystallographic data for **1–5**. These data can be obtained free of charge via http://www.ccdc.cam.ac.uk/conts/retrieving.html, or from the Cambridge Crystallographic Data Centre, 12 Union Road, Cambridge CB2 1EZ, UK; fax: (+44) 1223-336-033; or e-mail: deposit@ccdc.cam.ac.uk.

Supplementary data associated with this article can be found, in the online version, at http://dx.doi.org/10.1016/j.poly.2016.08.038.

References

[1] W.-L. Zhang, Y.-Y. Liu, J.-F. Ma, Cryst. Growth Des. 8 (2008) 1250.
[2] J.-Q. Liu, W.-P. Wu, Y.-Y. Wang, W.-H. Huang, W.-H. Zhang, Q.-Z. Shi, J.S. Miller, Inorg. Chim. Acta 362 (2009) 1295.
[3] V. Vo, Y. Kim, N.V. Minh, C.S. Hong, S.J. Kim, Polyhedron 28 (2009) 1150.
[4] (a) Q. Zhang, Q. Zhou, Y. Cheng, L. Wang, D. Ma, X. Jing, F. Wang, Adv. Mater. 16 (2004) 432;
(b) N. Armaroli, G. Accorsi, M. Holler, O. Moudam, J.-F. Nierengarten, Z. Zhou, R.T. Wegh, R. Welter, Adv. Mater. 18 (2006) 1313;
(c) Q. Zhang, Q. Zhou, Y. Cheng, L. Wang, D. Ma, X. Jing, F. Wang, Adv. Funct. Mater. 16 (2006) 1203;
(d) T. MacCormick, W.-L. Jia, S. Wang, Inorg. Chem. 45 (2006) 147;
(e) H. Ge, W. Wei, P. Shuai, G. Lei, S.J. Qing, J. Lumin. 131 (2011) 238.
[5] (a) D.G. Cuttell, S.-M. Kuang, P.E. Fanwick, D.R. McMillin, R.A. Walton, J. Am. Chem. Soc. 124 (2002) 6;
(b) P. Coppens, Chem. Commun. (2003) 1317;
(c) P. Coppens, I.I. Vorontsov, T. Graber, A.Y. Kovalevsky, Y.-S. Chen, G. Wu, M. Gembicky, I.V. Novozhilova, J. Am. Chem. Soc. 126 (2004) 5980;
(d) K. Saito, T. Arai, N. Takahashi, T. Tsukuda, T. Tsubomura, Dalton Trans. (2006) 4444;
(e) C.L. Linfoot, P. Richardson, T.E. Hewat, O. Moudam, M.M. Forde, A. Collins, F. White, N. Robertson, Dalton Trans. 39 (2010) 8945;
(f) R.D. Costa, D. Tordera, E. Orti, H. Bolink, J. Schönle, S. Graber, C.E. Housecroft, E.C. Constable, J.A. Zampese, J. Mater. Chem. 21 (2011) 16108.
[6] (a) N. Armaroli, G. Accorsi, G. Bergamini, P. Ceroni, M. Holler, O. Moudam, C. Duhayon, B. Delavaux-Nicot, J.-F. Nierengarten, Inorg. Chim. Acta 360 (2007) 1032;
(b) A. Listorti, G. Accorsi, Y. Rio, N. Armaroli, O. Moudam, A. Gégout, B. Delavaux-Nicot, M. Holler, J.-F. Nierengarten, Inorg. Chem. 47 (2008) 6254;
(c) M. Mohankumar, M. Holler, J.-F. Nierengarten, J.-P. Sauvage, Chem. Eur. J. 18 (2012) 12192;
(d) M. Mohankumar, M. Holler, M. Schmitt, J.-P. Sauvage, J.-F. Nierengarten, Chem. Commun. 49 (2013) 1261.
[7] A. Kaeser, M. Mohankumar, J. Mohanraj, F. Monti, M. Holler, J.-J. Cid, O. Moudam, I. Nierengarten, L. Karmazin-Brelot, C. Duhayon, B. Delavaux-Nicot, N. Armaroli, J.-F. Nierengarten, Inorg. Chem. 52 (2013) 12140.
[8] Adrien Kaeser, Béatrice Delavaux-Nicot, Carine Duhayon, Yannick Coppel, Jean-François Nierengarten, Inorg. Chem. 52 (2013) 14343.
[9] M.C. Gimeno, P.G. Jones, A. Laguna, C.J. Sarroca, Dalton Trans. (1995) 1473.
[10] (a) E. Bembenek, O. Crespo, M.C. Gimeno, P.G. Jones, A. Laguna, J. Chem. Ber. 127 (1994) 835;
(b) O. Crespo, M.C. Gimeno, P.G. Jones, A. Laguna, J. Chem. Soc., Dalton Trans. 24 (1996) 4583.
[11] T.S. Andy Hor, Inorg. Chim. Acta 149 (1988) 157.
[12] A. Cingolani, Effendi, F. Marchetti, C. Pettinari, R. Pettinari, B.W. Skelton, A.H. White, Inorg. Chim. Acta 329 (2002) 100.
[13] (a) Effendy, J.V. Hanna, F. Marchetti, D. Martini, C. Pettinari, R. Pettinari, B.W. Skelton, A.H. White, Inorg. Chim. Acta 357 (2004) 1523;
(b) Effendy, C. Di Nicola, M. Nitiatmodjo, C. Pettinari, B.W. Skelton, A.H. White, Inorg. Chim. Acta 358 (2005) 735;
(c) Effendy, C. Di Nicola, M. Fianchini, C. Pettinari, B.W. Skelton, N. Somers, A. H. White, Inorg. Chim. Acta 358 (2005) 763;
(d) A. Cingolani, Effendy, C. Pettinari, B.W. Skelton, A.H. White, Inorg. Chim. Acta 359 (2006) 2170;
(e) Effendy, F. Marchetti, C. Pettinari, R. Pettinari, B.W. Skelton, A.H. White, Inorg. Chim. Acta 360 (2007) 1388.
[14] C.J. Jones, Chem. Soc. Rev. 27 (1998) 289.
[15] M.W. Hosseini, Acc. Chem. Res. 38 (2005) 313.
[16] D. Bradshow, J.B. Claridge, E.J. Cussen, T.J. Prior, M.J. Rosseinsky, Acc. Chem. Res. 38 (2005) 273.
[17] H. Lee, T.H. Noh, O.-S. Jung, CrystEngComm 15 (2013) 1832.
[18] O.-S. Jung, Y.J. Kim, Y.-A. Lee, J.K. Park, H.K. Chae, J. Am. Chem. Soc. 122 (2000) 9921.
[19] (a) P. Blondeau, A. van der Lee, M. Barboiu, Inorg. Chem. 44 (2005) 5649;
(b) J.L. Sague, M. Meuwly, K.M. Fromm, CrystEngComm 10 (2008) 1542;
(c) M. Wenzel, K. Wichmann, K. Gloe, K. Gloe, H.-J. Buschmann, K. Otho, M. Schröder, A.J. Blake, C. Wilson, A.M. Mills, L.F. Lindoy, P. Plieger, CrystEngComm 12 (2010) 4176;
(d) D.L. Reger, A. Leitner, P.J. Pellechia, M.D. Smith, Inorg. Chem. 53 (2014) 9932.
[20] W. Sabina, M. Jaros, C. Fátima, Guedes da Silva, Magdalena Florek, M. Conceição Oliveira, Piotr Smoleński, Armando J.L. Pombeiro, Alexander M. Kirillov, Cryst. Growth Des. 14 (2014) 5408.
[21] Piotr Smoleński, Claudio Pettinari, Fabio Marchetti, M. Fátima C. Guedes da Silva, Giulio Lupidi, Gretta Veronica Badillo Patzmay, Dezemona Petrelli, Luca A. Vitali, Armando J.L. Pombeiro, Inorg. Chem. 54 (2015) 434.
[22] M.C. Beard, G.M. Turner, C.A. Schmuttenmaer, Phys. Rev. B: Condens. Matter 19 (2003) 23.
[23] R.D. Averitt, G. Rodriguez, J.L.W. Siders, J. Opt. Soc. Am. B 17 (2000) 327.
[24] M. Nagel, P.H. Bolivar, M. Brucherseifer, H. Kurz, A. Bosserhoff, R. Buttner, Appl. Opt. 41 (2002) 2074.
[25] M. Seel, S. Engleitner, W. Zinth, Chem. Phys. Lett. 275 (1997) 363.
[26] Qiong-Hua Jin, Yuan Yuan, Yu-Ping Yang, Qi-Ming Qiu, Min Liu, Zhong-Feng Li, Zhen-Wei Zhang, Cun-Lin Zhang, Polyhedron 101 (2015) 56.
[27] Yuan Yuan, Xiao-Nan Xue, Wei-Wei Fan, Qi-Ming Qiu, Yang-Zhe Cui, Min Liu, Zhong-Feng Li, Qiong-Hua Jin, Yu-Ping Yang, Zhen-Wei Zhang, Wen-Xiao Geng, Wen-Jie Zheng, Polyhedron 106 (2016) 178.
[28] S. Xu, M. Liu, Y.-P. Yang, Y.-H. Jiang, Z.-F. Li, Q.-H. Jin, X. Wang, X.-N. Xue, Polyhedron 87 (2015) 293.
[29] L.-L. Zhang, H. Zhong, C. Deng, C.-L. Zhang, Y.-J. Zhao, Appl. Phys. Lett. 94 (2009) 211106.
[30] Indian Pharmacopoeia (Ministry of Health and Family Welfare New Delhi) (1996) A-114.
[31] A. Jarrahpour, D. Khalili, E. De Clercq, C. Salmi, J.M. Brunel, Molecules 12 (2007) 1720.
[32] T. Hu, Thomas, C.W. Mak, Cryst. Growth Des. 13 (2013) 4957.
[33] Y.H. Wang, K.L. Chu, H.C. Chen, C.W. Yeh, Z.K. Chan, M.C. Suen, J.D. Chen, J.C. Wang, Cryst. Eng. Commun. 8 (2006) 84.
[34] Effendy, Fabio Marchettic, Claudio Pettinaric, Riccardo Pettinaric, Brian W. Skeltona, Allan H. White, Inorg. Chim. Acta 360 (2007) 1414.
[35] X.-X. Li, Y.-Q. Gong, H.-X. Zhao, R.-H. Wang, Inorg. Chem. 53 (2014) 12127–12134.
[36] X. Huang, Z.-F. Li, Q.-H. Jin, Q.-M. Qiu, Y.-Z. Cui, Q.-R. Yang, Polyhedron 65 (2013) 129.
[37] J. Huang, Z.-P. Deng, Y.-H. Xiao, L.-H. Huo, S.-N. Zhao, F.-Y. Ge, S. Gao, Dalton Trans. 44 (2015) 5837–5847.
[38] Q.-M. Qiu, M. Liu, Z.-F. Li, Q.-H. Jin, X. Huang, Z.-W. Zhang, C.-L. Zhang, Q.-X. Meng, J. Mol. Struct. 1062 (2014) 125.
[39] L.M. Yang, H.Q. Sun, S.F. Weng, K. Zhao, L.L. Zhang, G.Z. Zhao, Y.G. Wang, Y.Z. Xu, X.Y. Lu, C.L. Zhang, J.G. Wu, J.E. Chen, Spectrochim. Acta, Part A 69 (2008) 160.
[40] L.M. Yang, X.H. Hua, J.H. Xue, Q.H. Pan, L. Yu, W.H. Li, Y.Z. Xu, G.Z. Zhao, L.M. Liu, K.X. Liu, J. Chen, J.G. Wu, Inorg. Chem. 51 (2012) 499.
[41] X. Yang, X. Huang, Q.-M. Qiu, Q.-H. Jin, C.-L. Zhang, Acta. Crystallogr. E68 (2012) m1367.
[42] Q.-M. Qiu, X. Huang, Y.-H. Zhao, M. Liu, Q.-H. Jin, Z.-F. Li, Z.-W. Zhang, C.-L. Zhang, Q.-X. Meng, Polyhedron 83 (2014) 16.
[43] H. Zhang, G.L. Zhuang, X.J. Kong, Cryst. Growth Des. 13 (2013) 2493.